J. Plasma Phys. (2022), *vol*. 88, 905880605 © The Author(s), 2022.
Published by Cambridge University Press
doi:10.1017/S002237782200112X

Effect of sheared $E \times B$ flow on the blob dynamics in the scrape-off layer of HL-2A tokamak

W.C. Wang[1], J. Cheng[2,†], Z.B. Shi[1], L.W. Yan[1], Z.H. Huang[1], N. Wu[1], Q. Zou[2], Y.J. Zhu[2], X. Chen[2], J.Q. Dong[1,3], W.L. Zhong[1] and M. Xu[1]

[1]Southwestern Institute of Physics, Chengdu, Sichuan 610041, PR China

[2]Institute of Fusion Science, School of Physical Science and Technology, Southwest Jiaotong University, Chengdu 610031, PR China

[3]Institute for Fusion Theory and Simulation, Zhejiang University, Hangzhou 310027, PR China

(Received 31 May 2022; revised 23 September 2022; accepted 23 September 2022)

The effect of sheared $\boldsymbol{E \times B}$ flow on the blob dynamics in the scrape-off layer (SOL) of HL-2A tokamak has been studied during the plasma current ramp-up in ohmically heated deuterium plasmas by the combination of poloidal and radial Langmuir probe arrays. The experimental results indicate that the SOL sheared $\boldsymbol{E \times B}$ flow is substantially enhanced as the plasma current exceeds a certain value and the strong sheared $\boldsymbol{E \times B}$ flow has the ability to slow the blob radial motion via stretching its poloidal correlation length. The locally accumulated blobs are suggested to be responsible for the increase of plasma density just outside the Last Closed Flux Surface (LCFS) observed in this experiment. The results presented here reveal the significant role played by the strong sheared $\boldsymbol{E \times B}$ flow on the blob dynamics, which provides a potential method to control the SOL width by modifying the sheared $\boldsymbol{E \times B}$ flow in future tokamak plasmas.

Key words: turbulence, blob, $\boldsymbol{E \times B}$ shear flow, scrape-off layer, Langmuir probe

1. Introduction

Plasma transport in the scrape-off layer (SOL) has been widely accepted to be governed by the radial motion of blobs, which are characterized by a density higher than that of the background plasma and they extend along the magnetic field line (Krasheninnikov 2001; D'Ippolito, Myra & Krasheninnikov 2002; Zweben *et al.* 2003). The blobs provide a channel for the convective radial transport of particles and heat in the SOL region. (Terry *et al.* 2003; Garcia *et al.* 2007*a*; D'Ippolito, Myra & Zweben 2011). Therefore, studying how blob behaviour affects or determines the SOL width and peak heat load in fusion devices is important.

In recent years, blob generation (Bisai *et al.* 2005; Furno *et al.* 2008; Happel *et al.* 2009; Cheng *et al.* 2013), birth region (Myra *et al.* 2006*a*; Xu *et al.* 2009; Fuchert *et al.* 2016), radial propagation (Xu *et al.* 2005; Katz *et al.* 2008; Tsui *et al.* 2018) and the resultant convective transport (Garcia *et al.* 2004; Myra, Russell & D'Ippolito 2006*b*; Russell, Myra & D'Ippolito 2007; Offeddu *et al.* 2022) have been active research topics.

† Email address for correspondence: chengj@swjtu.edu.cn

Earlier simulation work demonstrated that the sheared $\boldsymbol{E} \times \boldsymbol{B}$ flow plays a crucial role in the turbulence transport (Burrell 1998) and can also stop the blob radial motion within the shear layer (Ghendrih *et al.* 2009). Recently, several theoretical studies (Halpern *et al.* 2017; Fedorczak *et al.* 2019; Giacomin *et al.* 2021) have derived models for the density or power decay widths in SOL, however, they do not explicitly include the effects of the sheared $\boldsymbol{E} \times \boldsymbol{B}$ flow. The experiments performed on TCV tokamak indicated that the main reason for the reduction of the blob radial velocity in the far-SOL region is the sheath dissipation with increasing plasma current (Garcia *et al.* 2007*b*). The multi-device (AUG, TCV and MAST) experimental results demonstrated that the variation of SOL width is related to the blob radial velocity characteristics (Kirk *et al.* 2016; Vianello *et al.* 2019), but the effects of the sheared $\boldsymbol{E} \times \boldsymbol{B}$ shear flow on the blob dynamics have not been explicitly evaluated. The recent work on AUG showed that the external generated sheared $\boldsymbol{E} \times \boldsymbol{B}$ flow via the radio-frequency heating enables the stretching, distortion and splitting of blobs in far-SOL regions (Zhang *et al.* 2019). The splitting and tilting of turbulent structures were observed in the strong $\boldsymbol{E} \times \boldsymbol{B}$ flow region in TEXTOR plasmas using gas puffing imaging (Shesterikov *et al.* 2012). However, the interplay between the $E \times B$ shear flow and turbulence is still not completely understood and requires further investigation.

In this work, we report the effect of sheared $\boldsymbol{E} \times \boldsymbol{B}$ flow on the blob dynamics during plasma current ramp-up in HL-2A ohmically heated deuterium plasmas. The experimental results illustrate that (i) the sheared $\boldsymbol{E} \times \boldsymbol{B}$ flow in the near-SOL region is significantly enhanced as plasma current exceeds a certain value; (ii) the blob radial motion is remarkably reduced due to the sheared $\boldsymbol{E} \times \boldsymbol{B}$ flow. The rest of this paper is organized as follows. Section 2 describes the experimental set-up. Section 3 presents the experiment results, including the experimental characterization of turbulence in the near-SOL region during the plasma current ramp-up. Finally, § 4 presents the conclusions and discussion.

2. Experimental set-up

Experiments were performed in the ohmically heated deuterium discharges of the HL-2A tokamak with limiter configurations. The typical experimental parameters were as follows: plasma current $I_p = 130$–170 kA, toroidal magnetic field $B_t = 1.7$–1.8 T and line-averaged density $n_{\mathrm{el}} = (1.1\text{–}1.4) \times 10^{19}$ m^{-3}. The two combined Langmuir probe arrays, illustrated in figure 1, were utilized to study the dynamical interactions of the sheared $\boldsymbol{E} \times \boldsymbol{B}$ flow and blobs during the plasma current ramp-up. The array A, localized approximately 21 mm below the mid-plane, is comprised of ten tips aligned in the poloidal direction (numbered 1–10 from the top to the bottom, the poloidal separation between adjacent tips being $\Delta d = 4$ mm). The arc-shaped poloidal array A was designed to make the tips align along the magnetic flux surface as much as possible. Radial arrays B and C, localized approximately 52 mm above and below the mid-plane, respectively, were used to measure the radial profiles of floating potentials and plasma density $\sim I_s$). A standard four-tip array (Lin *et al.* 1992; Tsui *et al.* 1992) with a biased voltage -180 V was specially placed at the SOL shearing layer region to measure blob potential and radial velocity, etc. In our experiment, the measured position of the four-tip probe is $\Delta r = +10$ mm, where the positive and negative signs of Δr denote the outside and inside of the Last Closed Flux Surface (LCFS), respectively. The approximate position of the LCFS was identified using an equilibrium fitting code (EFIT) with an accuracy of 5 mm. The plasma geometry, LCFS position and Grad–Shafranov shift remained almost unchanged during the plasma current ramp-up. The flux expansion along the flux surfaces was negligible in the poloidal range covered by array A during the discharge. The major and minor radii slightly varied throughout the discharge. The black arcthick line shown in figure 1(*c*) denotes the poloidal limiter. The data acquisition frequency was fs = 1 MHz with a resolution of 12 bits.

https://doi.org/10.1017/S002237782200112X Published online by Cambridge University Press

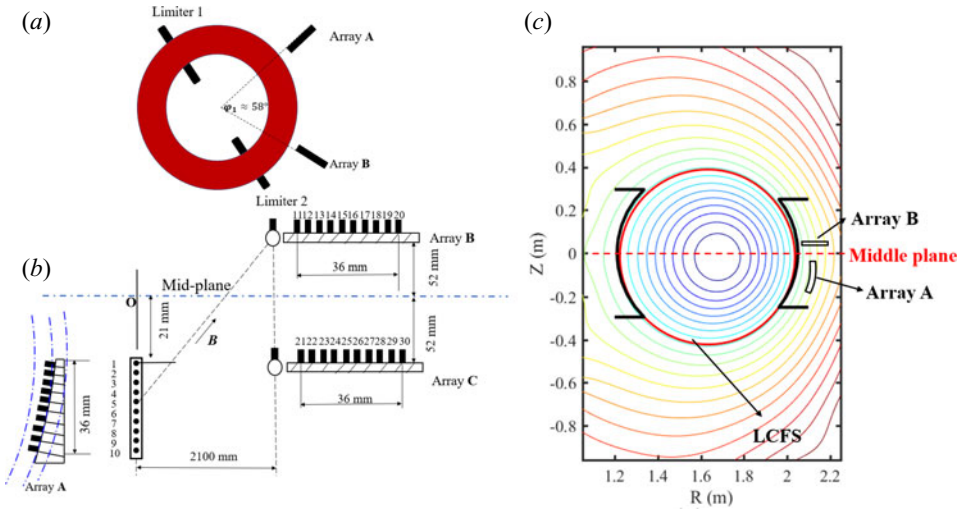

FIGURE 1. (*a*) Bird's eye view of Langmuir probe arrays in the toroidal direction; (*b*) schematic illustration of the poloidal and radial arrays of probes; (*c*) equilibrium configuration reconstructed by the EFIT code and the location of probe measurement (the thick solid black line represents the poloidal limiter).

The results presented herein are well reproducible. Figure 2 displays the time traces of the discharge parameters for one typical discharge (no. 12234) during the plasma current ramp-up from $I_p = 135$ to 172 kA within 900 ms, wherein the line-averaged density ($n_{\rm el}$) increases from 1.1×10^{19} to 1.4×10^{19} m^{-3}, approximately 25 %, and the corresponding Greenwald fraction was approximately unchanged, $n_{\rm el}/n_G = 0.43$–0.45, where $n_G = I_p/\pi a^2$, where a is the mirror radius. The electron temperature, density and the radial electric field were measured by the 4-tip probe localized at $\Delta r = +10$ mm. It was observed that both electron temperature and density obviously started to increase from $t = 850$ ms, while the radial electric field accordingly changed its sign from positive to negative as the plasma current exceeded $I_p = 150$ kA (black dashed line in figure 2). The plasma horizontal displacement represents the distance of LCFS away from the reference position at the middle plane, which was measured using two horizontal flux loops that were symmetrically arranged in the vacuum of the middle plane, ensuring the reliability of the probe measurement in this experiment. During this phase the plasma horizontal displacement was less than 3 mm.

3. Experimental results

3.1. *Spatio-temporal evolution of SOL parameters during plasma current ramp-up*

Figure 3 shows the time traces of the plasma current together with the spatio-temporal distribution of skewness, mean $E \times B$ shearing rate and the inverse scale of plasma density during the plasma current ramp-up (rise rate of 0.04 kA ms^{-1}). Skewness describes the asymmetry of the probability distribution function or the degree of deviation from a Gaussian distribution. Here, the skewness is calculated as $S = \langle \tilde{x}^3 \rangle / \langle \tilde{x}^2 \rangle^{3/2}$, where $\tilde{x}$ is the time series of the ion saturation current signals and is given in figure 3(*b*). It was seen that the sign of skewness is always positive in the SOL and is significantly reduced after $t = 850$ ms, suggesting the blob behaviour was dramatically suppressed. The mean $E \times B$

https://doi.org/10.1017/S002237782200112X Published online by Cambridge University Press

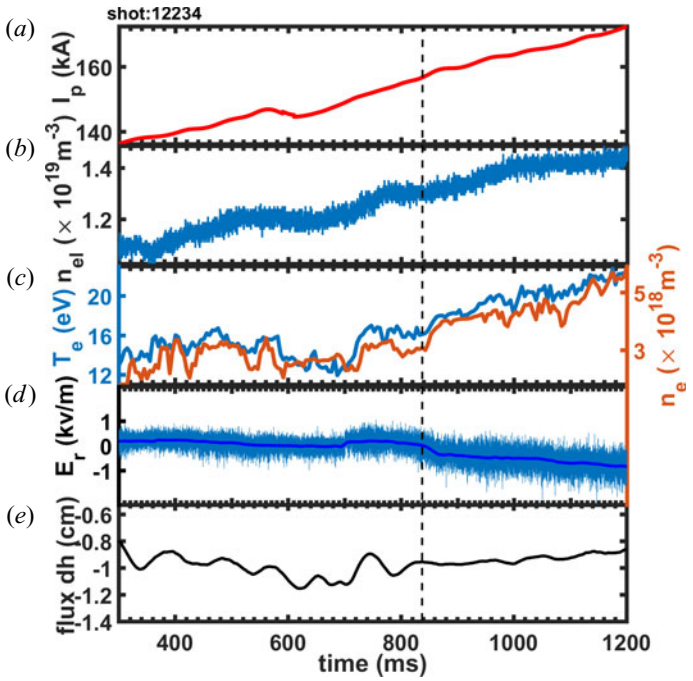

FIGURE 2. Time traces of the plasma current (*a*), the line-averaged density (*b*), the electron temperature and plasma density (*c*), the radial electric field (*d*) measured at $\Delta r = +10$ mm and the plasma horizontal displacement (*e*).

shearing rate is estimated as

$$\omega_{E\times B}(i) \approx \frac{1}{B_t}\frac{\partial^2 V_f}{\partial^2 r} = [V_f(i-1) - V_f(i+1) + 2V_f(i)]/(B_t \Delta d^2), \tag{3.1}$$

where i represents the probe number in the radial array ($i = 2$–9), V_f represents the floating potential and Δd denotes the radial separation of neighbouring tips. It should be pointed out that the radial electric field here was calculated by the derivative of the floating potential, neglecting the effect of the electron temperature gradient, due to the fact that the change in the electron temperature gradient is less pronounced in the SOL and the floating potential profiles were very nearly the same as those for the plasma potential in similar discharges. On the other hand, the inverse scale of the density gradient is expressed as

$$L_{\rm ne}^{-1} = -\nabla n_e/n_e = -\nabla(I_s\sqrt{T_e})/(I_s\sqrt{T_e}) = L_{\rm Is}^{-1} - 0.5L_{\rm Te}^{-1}. \tag{3.2}$$

The above formula can be rewritten as

$$\frac{L_{\rm ne}^{-1}}{L_{\rm Is}^{-1}} = 1\text{–}0.5\frac{L_{\rm ne}^{-1}}{L_{\rm Is}^{-1}} = 1\text{–}0.5\zeta, \tag{3.3}$$

where $L_{\rm ne}^{-1}$ and $L_{\rm Is}^{-1}$ represent the inverse scale of the density and ion saturation current, and $\zeta = L_{\rm Te}^{-1}/L_{\rm Is}^{-1}$ is approximately 0.12∼0.16 in HL-2A near-SOL region ($\Delta r = 5$–15 mm), i.e. $L_{\rm ne}^{-1}/L_{\rm Is}^{-1} \approx 0.92$–$0.94 \approx 1$. Therefore, the estimated $L_{\rm Is}^{-1}$ could be considered as the proxy of $L_{\rm ne}^{-1}$ in this region. Figure 3(*c*) shows the spatio-temporal distributions

https://doi.org/10.1017/S002237782200112X Published online by Cambridge University Press

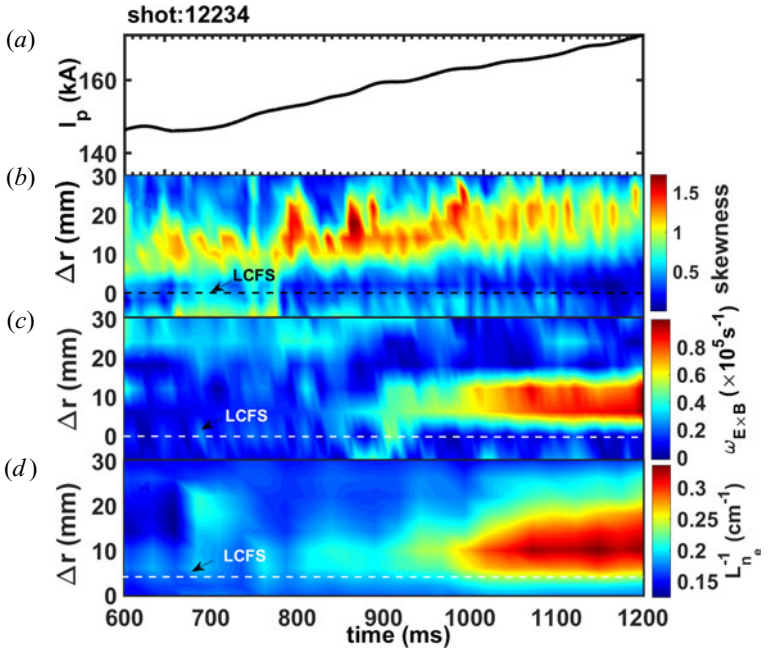

FIGURE 3. The temporal evolutions of the plasma current (*a*), the spatio-temporal distributions of skewness (*b*), $\boldsymbol{E \times B}$ shearing rate (*c*) and the inverse scale of density gradient (*d*).

of the $\boldsymbol{E \times B}$ shearing rate, where it is seen that a 10 mm-width $\boldsymbol{E \times B}$ shearing layer is significantly formed just outside the LCFS as the plasma current exceeds 155 kA at t = 850 ms, meanwhile, the local density gradient also obviously rises, as seen in figure 3(*d*). The observed results indicate the presence of a potential relation between the strong sheared $\boldsymbol{E \times B}$ flow and localized density gradient. Similar experiment results were reported in the EAST H-mode plasmas (Yang *et al.* 2015).

To further clarify the underlying physics, we compared the radial variations of the skewness, the inverse scale of the density gradient, the $\boldsymbol{E \times B}$ shearing rate and ion saturation current (a proxy of density, $I_s \propto n_e$) in two scenarios with low ($I_p = 155$ kA) and high ($I_p = 170$ kA) plasma currents and the results are presented in figure 4. As shown in figure 4(*a*), the skewness measured at near-SOL region (denoted by the shaded area) substantially decreases in the high I_p case ($I_p = 170$ kA) compared with that in low I_p case ($I_p = 155$ kA), implying the intermittent blob behaviour is significantly suppressed in the high current case. Meanwhile the $\boldsymbol{E \times B}$ shearing rate dramatically rises, as seen in figure 4(*b*), reflecting the presence of the local $\boldsymbol{E \times B}$ shearing layer. In addition, the local density gradient also increases in the region where the $\boldsymbol{E \times B}$ shearing layer was formed, as illustrated in figure 4(*c*). Here, note that SOL turbulence is dominated by intermittent blobs, which might play a significant role in SOL density profile (Garcia *et al.* 2007*c*; Carralero *et al.* 2015; Militello & Omotani 2016; Vianello *et al.* 2019). These observed results therefore indicated that the enhanced $\boldsymbol{E \times B}$ shear flow may play a predominant role in blob behaviours and the resulting density profile in the SOL.

3.2. *Dynamics of blob behaviours in the near-SOL region*

3.2.1. *Blob stretched by the strong sheared E × B flow*

The cross-correlation function (CCF) was utilized to reconstruct a two-dimensional (2-D) coherent structure depending on the significant long-range correlation along the

https://doi.org/10.1017/S002237782200112X Published online by Cambridge University Press

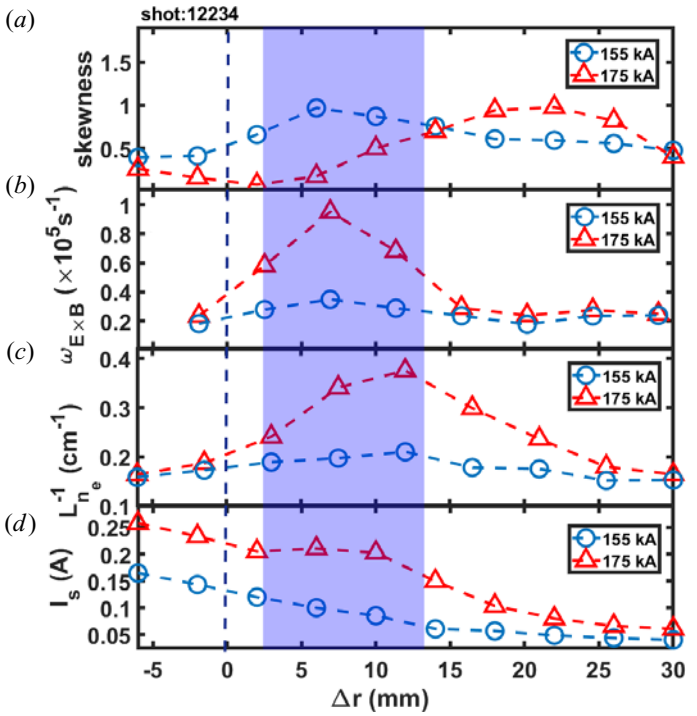

FIGURE 4. Comparison of radial profiles of skewness (*a*), $\boldsymbol{E} \times \boldsymbol{B}$ shearing rates (*b*), the inverse scale of density gradient (*c*) and ion saturation current ($I_s \propto n_e$) (*d*) (the vertical line represents the approximate position of the LCFS).

same magnetic field line (Grulke *et al.* 2001; Cheng *et al.* 2013). A region with poloidal–radial dimensions of 36 × 36 mm^2 was established with the combined poloidal (array A) and radial (array B) probe arrays that were toroidally separated by $L_\varphi =$ 2100 mm. The CCF was computed from two types of ion saturation signals: the reference signal $S_x(i)$ was obtained from the poloidal array A ($1 \le i \le 10$) and $S_y(i)$ was obtained from the radial array B ($11 \le j \le 20$), where i and j denote the probe positions in the poloidal and radial probe arrays, respectively, as sketched in figure 1. The correlation coefficient of the CCF was estimated at zero time lag and placed at the point in the matrix, i.e. $\gamma_{\max}(i, j)$. Following this method, the contour of the correlations was obtained. The calculated matrix displays a contour for the 2-D image of the coherent structure. Figures 5(*a*)–5(*c*) display the 2-D images of the coherent structure with different sheared $\boldsymbol{E} \times \boldsymbol{B}$ flows. The blob poloidal correlation length for the three different $\boldsymbol{E} \times \boldsymbol{B}$ shearing rates was roughly estimated as 0.5 cm, 1.1 cm and 1.5 cm by the e-folding decay spatial scale of the CCF, which is qualitatively consistent with the results estimated by two-point correlation method (Beall, Kim & Powers 1982) $L_c = 1/\langle\sigma_k\rangle$, where $\langle\sigma_k^2\rangle = \sum_f [\sum_k [k - \bar{k}(f)]^2 \cdot s(k|f)]$, $s(f)$ denotes the spectral density, f and k denote the frequency and wavenumber, respectively. It was found that the blob poloidal correlation length was increased by approximately three times whereas the radial correlation length has less pronounced change as the $\boldsymbol{E} \times \boldsymbol{B}$ sheared flow rises from $\omega_{E\times B} = 0.12 \times 10^5$ to 1.08×10^5 s^{-1}, implying that strong $\boldsymbol{E} \times \boldsymbol{B}$ shear flow has an ability to stretch coherent structures. A similar experimental result has been reported in other devices (Carter & Maggs 2009). Here, we compare theoretical predictions of critical velocity shear with

https://doi.org/10.1017/S002237782200112X Published online by Cambridge University Press

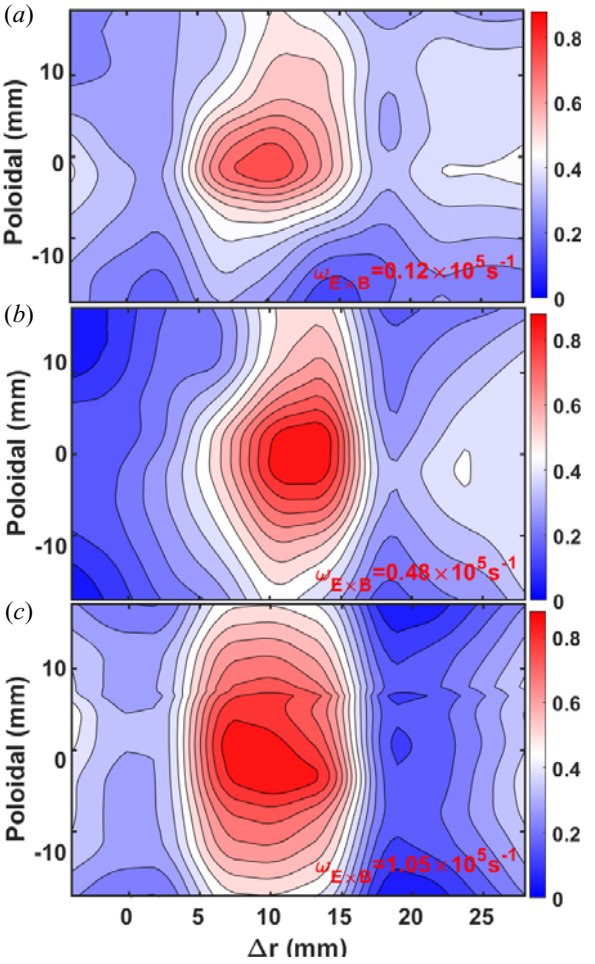

FIGURE 5. Contour plot of the coherence between array A and array B toroidally separated by 2100 mm for different $\boldsymbol{E \times B}$ shearing rates $\omega_{E\times B} = 0.12 \times 10^5$ s^{-1} (*a*), $\omega_{E\times B} = 0.48 \times 10^5$ s^{-1} (*b*) and $\omega_{E\times B} = 1.08 \times 10^5$ s^{-1} (*c*).

experimental observations reported in this work. According to the theoretical prediction (Yu & Krasheninnikov 2003), the magnitude (Φ^{crit}) of critical potential was calculated as $\Phi^{\text{crit}} = T_e \cdot \Phi^{\text{crit}}_{\text{nor}}/e$, where T_e represents electronic tempreture, e is elementary charge and $\Phi^{\text{crit}}_{\text{nor}}$ means the normalized magnetite of potential related to the critical velocity shear, which could be addressed as $\Phi^{\text{crit}}_{\text{nor}} = (\delta_s/2\rho_s)^3(\delta_b/L)$, where $\rho_s \approx 0.046$ cm, connection length $L \approx 2.1 \times 10^3$ cm, blob size $\delta_b \approx 1.6$ cm and width of $E \times B$ shear layer $\delta_s \approx 1.0$ cm, where ρ_s is Larmer radius. Using the plasma parameters $T_e \approx$ 18 eV $\Phi^{\text{crit}}_{\text{nor}} \approx 0.98$, the estimated magnitude Φ^{crit} was about 17.6 V, which is very close to the experimental observation ≈15 V.

The statistical distribution of the blob poloidal correlation lengths against the blob amplitudes with different $\boldsymbol{E \times B}$ shearing rates was analysed and presented in figure 6. It was clearly seen that the blob poloidal correlation length monotonically rises with increasing $\boldsymbol{E \times B}$ shearing rate for different blob amplitudes. An interesting observation here is that the maximum variation of the poloidal correlation length for large blobs

https://doi.org/10.1017/S002237782200112X Published online by Cambridge University Press

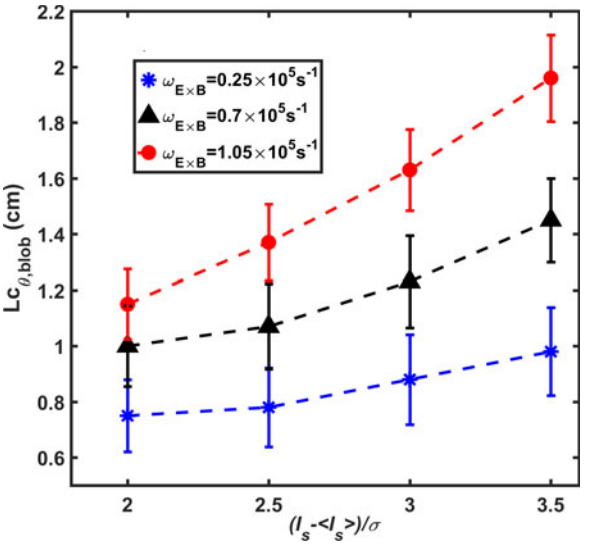

FIGURE 6. Statistical analysis of blob poloidal correlation length as a function of blob amplitude for the different $\boldsymbol{E \times B}$ shearing rates $\omega_{E\times B}$. The probe measurement is localized at $\Delta r = +10$ mm.

(3.5σ) occurred in the strong $\boldsymbol{E \times B}$ sheared flow case ($\omega_{E\times B} = 1.05 \times 10^5$ s^{-1}). Here, it should be pointed out that the estimated $\boldsymbol{E \times B}$ shearing rate is slightly lower than the blob decorrelation rate $1/\tau_c \approx 1.1 \times 10^5$ s^{-1} (where τ_c represents the blob lifetime inferred from the full width at half-maximum magnitude), concluding that blobs were not torn up by the $\boldsymbol{E \times B}$ flow (only stretching blobs). A similar experimental result on the blob stretched by the radio-frequency induced sheared flow in far SOL has been reported by (Zhang *et al.* 2019). In fact, a strong enough sheared $\boldsymbol{E \times B}$ flow via biasing can directly split the edge turbulent eddy structure and consequently cause the confinement improvement evidenced in TEXTOR (Shesterikov *et al.* 2012).

3.2.2. *Blobs deceleration due to the poloidal elongation*

Conditional average was widely used to extract coherent structure from a turbulent signal in fusion plasmas and is generally defined as

$$y_{\mathrm{cond}}(\tau) = \frac{1}{N}\sum_{i=1}^{N}[y(t_i+\tau)|x(t_i) = \phi_c], \tag{3.4}$$

where $x(t)$ is the reference signal and $y(t)$ is the analysed signal. When the pre-set condition is met, the time t, becomes the reference time $\tau = 0$, and a subset from the analysed signal is taken around $\tau = 0$, from $-\tau_{\max}$ to $\tau_{\max}$. After searching the full reference signal for N occurrences of the condition, ϕ_c, a set of N waveforms from the analysed signal are assembled. This set is then ensemble averaged to give the conditional average for the condition ϕ_c (Filippas *et al.* 1995). In our analysis, the threshold $+2.5\sigma$ is used to detect the blobs. In cross-conditional average (CCA) analysis, the ion saturation current (as a proxy of plasma density) was routinely chosen as the reference signal. The conditional average was obtained by recording 120 data points (window length) around the maximum of each burst event, i.e. [-60 μs, $+60$ μs], and then accumulating and averaging the selected events.

https://doi.org/10.1017/S002237782200112X Published online by Cambridge University Press

Blob radial motion is widely accepted to be driven by the $\boldsymbol{E} \times \boldsymbol{B}$ formed within blobs (Krasheninnikov 2001), which is expressed as

$$\tilde{V}_r^{\text{blob}} = \tilde{E}_{\theta,\text{blob}}/B_t = (\tilde{V}_{f,\text{blob}}/Lc_{\theta,\text{blob}})B_t^{-1}, \tag{3.5}$$

where $\tilde{V}_{f,\text{blob}}$ represents the interior potential difference within the correlation length $Lc_{\theta,\text{blob}}$. The blob radial velocity ($\tilde{V}_r^{\text{blob}}$) was estimated with the reference signal (I_s) based on the CCA with $> 2.5\sigma$ thresholds. Furthermore, it is generally observed that the floating potential in the blob has a dipole structure. Here, $\Delta V_{f,\text{blob}}$ and $Lc_{\theta,\text{blob}}$ are both key parameters for determining blob radial motion, and they are affected by numerous factors (Labombard *et al.* 2001) such as collisionality, spin and the sheared $\boldsymbol{E} \times \boldsymbol{B}$ flow. To clarify the inherent physics governing the blob dynamics, we computed the radial velocity and floating potentials of blobs ($>2.5\sigma$) measured at $\Delta r = +10$ mm, where the $\boldsymbol{E} \times \boldsymbol{B}$ shearing rate $\omega_{E\times B}$ changes from 0.15×10^5 to 1.0×10^5 s^{-1} and internal potential compared has less change in figure 7. It was found that the blob radial velocity gradually decreased from 1.63 km s^{-1} to 0.82 km s^{-1}, whereas the potential difference inside blobs stayed almost unchanged when the local $\boldsymbol{E} \times \boldsymbol{B}$ shearing rate was increased, as sketched in figure 7(*b*). Here, the plasma collisionality was estimated to be $v_{\text{ei}}^* \approx 20$–$23$ ($v_{\text{ei}}^* = L_\parallel/\lambda_{\text{ei}} \approx 10^{-16} L_\parallel n_e T_e^{-2}$, where $L_\parallel$ denotes magnetic correlation length) during the plasma current ramp-up from 155 to 175 kA, the less prominent variation of v_{ei}^* reflects that the effect of plasma collisionality on the potential could be negligible. These observed results indicate that the reduction of the blob radial velocity is mainly due to its poloidal elongation ($Lc_{\theta,\text{blob}}$). This is direct experimental evidence of the significant role played by the sheared $\boldsymbol{E} \times \boldsymbol{B}$ flow in blob radial motion via the poloidal elongation.

3.3. *Localized density gradient possibly effected by blob radial motion*

To study the potential effect of blob radial motion on the localized density gradient, we present the time trace of the $\boldsymbol{E} \times \boldsymbol{B}$ shearing rate together with the normalized density fluctuation, the blob radial velocity as well as the density gradient in figure 8. The four-tip probe localized at the outer-mid plane ($\Delta r \approx +10$ mm) was used to measure the normalized density fluctuation and blob radial velocity. Each point was estimated with approximately 20 ms data, and the red shaded area denotes the error bar calculated with the standard deviation as $(i) = \sqrt{(1/(N-1))\sum_{i=1}^{N}(x_i - \bar{x})^2}$, were x_i denotes the time series of the signal. It was found that the significant change of the $\boldsymbol{E} \times \boldsymbol{B}$ sheared rate occurs at about $t = 850$ ms, however, the normalized density fluctuation has a less pronounced variation as compared in figure 9(*a*), suggesting that the increased $E \times B$ sheared flow has no significant effect on the ambient turbulence in this region. On the other hand, the localized density gradient actually starts to dramatically rise from $t = 850$ ms, while the blob radial velocity accordingly reduces. These observed results reveal the crucial role played by the blob radial motion in the localized density gradient.

To obtain the statistical relation between localized density gradient and blob radial velocity, we have chosen a series of discharges with different SOL $\boldsymbol{E} \times \boldsymbol{B}$ shearing rates. All the discharges were ohmically heated plasmas with similar parameters including B_t and the line-averaged density (n_{el}). The probe measure position is localized at the near SOL, $\Delta r = +10$ mm. Figure 9 plots the blob radial velocity ($\tilde{V}_r^{\text{blob}}$) and the inverse scale of density gradient ($L_{n_e}^{-1}$) against the $\boldsymbol{E} \times \boldsymbol{B}$ shearing rate ($\omega_{E\times B}$). It is seen that the $\tilde{V}_r^{\text{blob}}$ monotonically decreases, whereas the density gradient increases as the SOL localized $\boldsymbol{E} \times \boldsymbol{B}$ shearing rate gradually rises from 0.6×10^5 to 1.1×10^5 s^{-1}. These observations suggest that a strong $\boldsymbol{E} \times \boldsymbol{B}$ sheared flow has a pronounced impact on slowing the blob

https://doi.org/10.1017/S002237782200112X Published online by Cambridge University Press

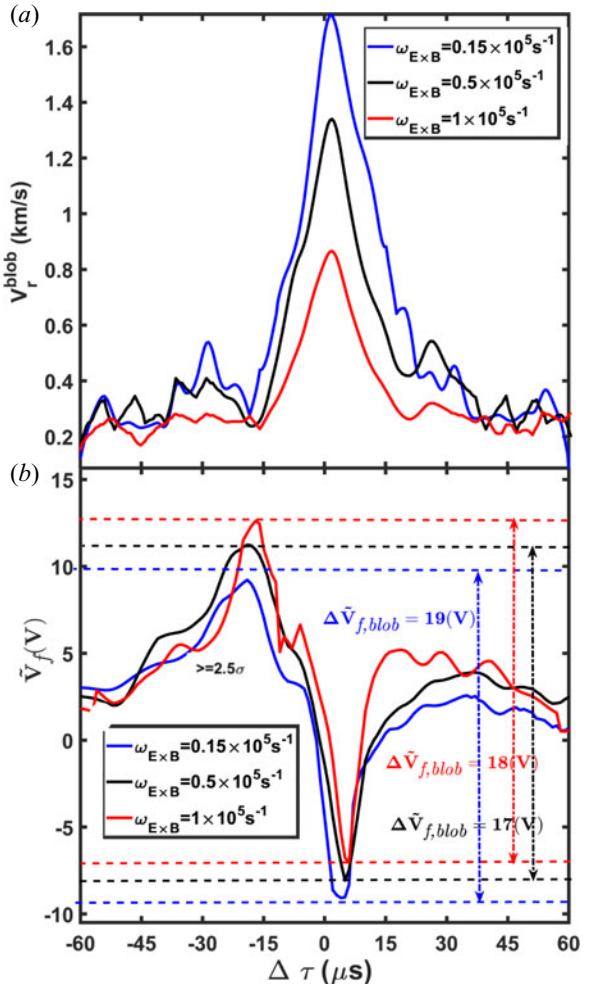

FIGURE 7. Comparison of blob radial velocity (*a*) and its internal potential (*b*) with amplitude $>2.5\sigma$ estimated by CCA in the scenarios with different $\boldsymbol{E}\times\boldsymbol{B}$ flow shearing rates $\omega_{E\times B}$. The measured radial position is at $\Delta r = +10$ mm.

radial motion, which was suggested to be related to the increased density observed in this experiment.

4. Conclusions

In summary, the effect of strong sheared $\boldsymbol{E}\times\boldsymbol{B}$ flow on the blob dynamics in the SOL of HL-2A tokamak has been studied during the plasma current ramp-up by combined Langmuir probe arrays. The experimental results demonstrated that a localized sheared $\boldsymbol{E}\times\boldsymbol{B}$ flow is dramatically enhanced as plasma current exceeds a certain value and it has the ability to slow the blob radial motion via stretching its poloidal correlation length. The localized accumulation of abundant blobs was believed to be responsible for the increase of plasma density just outside the LCFS. To our knowledge, this is direct experimental evidence of the interaction between the localized strong sheared $\boldsymbol{E}\times\boldsymbol{B}$ flow and blobs in the SOL. This study provides a potential method for controlling the SOL width by modifying the $\boldsymbol{E}\times\boldsymbol{B}$ flow in tokamak plasmas.

https://doi.org/10.1017/S002237782200112X Published online by Cambridge University Press

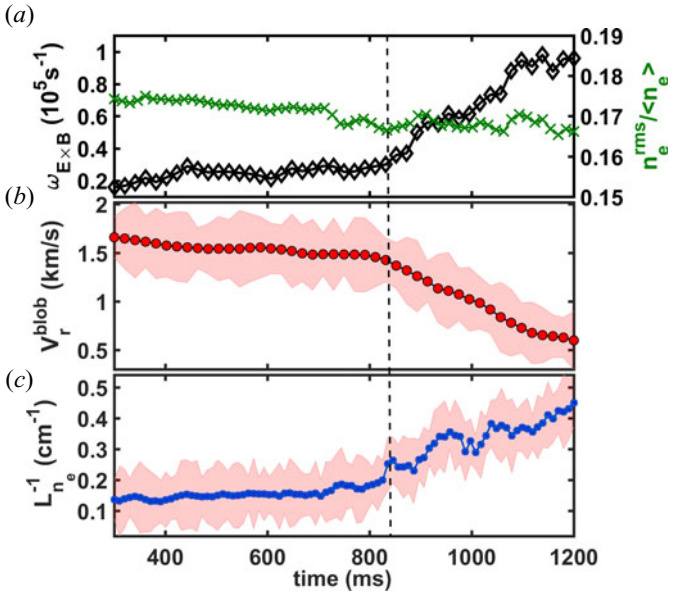

FIGURE 8. The time traces of the $\boldsymbol{E} \times \boldsymbol{B}$ flow shearing rate together with normalized density fluctuation (*a*), the blob radial velocity ($> 2.5\sigma$) (*b*) and the inverse scale length of density gradient (*c*), The probe measurement position is approximately localized at $\Delta r = +10$ mm.

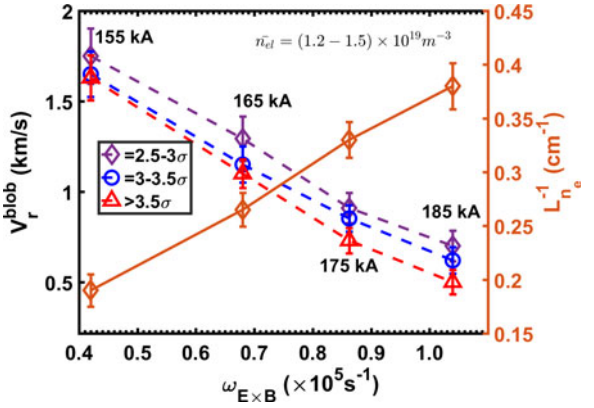

FIGURE 9. Blob radial velocity and density gradient against the $\boldsymbol{E} \times \boldsymbol{B}$ shearing rate. The measure radial position is at the normalized radial position at $\Delta r = +10$ mm.

However, some issues remain to be discussed. First, the radial electric field outside the LCFS might be determined by the sheath potential or other factors, the formation of the SOL shear layer and its possible dependence of the plasma current threshold has not yet been well understood, which is left for future study. Second, the SOL collisionality has less pronounced variation, as demonstrated in our experiment during the plasma current ramp-up, mainly due to the simultaneous increase of the plasma density and plasma current, we therefore ruled out the role of collisionality in the blob dynamics in this shearing flow layer region. It is not clear whether the collisionality has a significant effect on the blob radial motion in the far SOL. The detailed physics of the blob dynamics affected by the localized sheared flow will require study in future experiments.

https://doi.org/10.1017/S002237782200112X Published online by Cambridge University Press

Acknowledgements

Editor Hartmut Zohm thanks the referees for their advice in evaluating this article.

Funding

This work was supported by the National Science Foundation of China (grant number 12175186, 11875017, 11875020, 11820101004 and 11905052); the Sichuan Outstanding Youth Science Foundation (grant number 2020JDJQ0019); the Sichuan International Science and Technology Innovation Cooperation Project (grant number 2021YFH0066); the National Key R&D Program China (grant number 2019YFE03040002, 2022YFE03070001 and 2019YFE03090400) and Natural Science Foundation of Sichuan Province (grant number 2022NSFSC1820).

Declaration of interests

The authors report no conflict of interest.

REFERENCES

Beall, J.M., Kim, Y.C. & Powers, E.J. 1982 Estimation of wavenumber and frequency spectra using fixed probe pairs. *J. Appl. Phys*. **53**, 3933.

Bisai, N., Das, A., Deshpande, S., Jha, R., Kaw, P., Sen, A. & Singh, R. 2005 Formation of a density blob and its dynamics in the edge and the scrape-off layer of a tokamak plasma. *Phys. Plasmas* **12**, 102515.

Burrell, K.H. 1998 Turbulence and sheared flow. *Science* **281**, 1816.

Carralero, D., Manz, P., Aho-Mantila, L., Birkenmeier, G., Brix, M., Groth, M., Müller, H.W., Stroth, U., Vianello, N., Wolfrum, E., ASDEX Upgrade team & JET Contributors 2015 Experimental validation of a filament transport model in turbulent magnetized plasmas. *Phys. Rev. Lett*. **115**, 215002.

Carter, T.A. & Maggs, J.E. 2009 Modifications of turbulence and turbulent transport associated with a bias-induced confinement transition in the large plasma device. *Phys. Plasmas* **16**, 012304.

Cheng, J., Dong, J.Q., Yan, L.W., Itoh, K., Zhao, K.J., Hong, W.Y., Huang, Z.H., Nie, L., Lan, T. & Liu, A.D. 2013 Generation of large-scale coherent structures by turbulence in the edge plasmas of the HL-2A tokamak. *Nucl. Fusion* **53**, 093008.

D'Ippolito, D.A., Myra, J.R. & Krasheninnikov, S.I. 2002 Cross-field blob transport in tokamak scrape-off-layer plasmas. *Phys. Plasmas* **9**, 222.

D'Ippolito, D.A., Myra, J.R. & Zweben, S.J. 2011 Convective transport by intermittent blob-filaments: comparison of theory and experiment. *Phys. Plasmas* **18**, 060501.

Fedorczak, N., Peret, M., Bufferand, H., Ciraolo, G., Ghendrih, P. & Tamain, P. 2019 A spectral filament model for turbulent transport and scrape off layer width in circular geometry. *Nucl. Mater. Energy* **19**, 433.

Filippas, A.V., Bengston, R.D., Li, G.X., Meier, M., Ritz, C.P. & Powers, E.J. 1995 Conditional analysis of floating potential fluctuations at the edge of the Texas Experimental Tokamak Upgrade (TEXT-U). *Phys. Plasmas* **2**, 839.

Fuchert, G., Birkenmeier, G., Ramisch, M. & Stroth, U. 2016 Characterization of the blob generation region and blobby transport in a stellarator. *Plasma Phys. Control. Fusion* **58**, 054005.

Furno, I., Labit, B., Podesta, M., Fasoli, A., Mueller, S.H., Poli, F.M., Ricci, P., Theiler, C., Brunner, S. & Diallo, A. 2008 Experimental observation of the blob-generation mechanism from interchange waves in a plasma. *Phys. Rev. Lett*. **100**, 055004.

Garcia, O.E., Horacek, J., Pitts, R.A., Nielsen, A.H., Fundamenski, W., Naulin, V. & Rasmussen, J.J. 2007*a* Fluctuations and transport in the TCV scrape-off layer. *Nucl. Fusion* **47**, 667.

Garcia, O.E., Naulin, V., Nielsen, A.H. & Rasmussen, J.J. 2004 Computations of intermittent transport in scrape-off layer plasmas. *Phys. Rev. Lett*. **92**, 165003.

GARCIA, O.E., PITTS, R.A., HORACEK, J., MADSEN, J., NAULIN, V., NIELSEN, A.H. & RASMUSSEN, J.J. 2007*b* Collisionality dependent transport in TCV SOL plasmas. *Plasma Phys. Control. Fusion* **49**, B47.

GARCIA, O.E., PITTS, R.A., HORACEK, J., NIELSEN, A.H., FUNDAMENSKI, W., GRAVES, J.P., NAULIN, V. & RASMUSSEN, J.J. 2007*c* Turbulent transport in the TCV SOL. *J. Nucl. Mater.* **363-365**, 575.

GHENDRIH, P., CIRAOLO, G., LARMANDE, Y., SARAZIN, Y., TAMAIN, P., BEYER, P., CHIAVASSA, G., DARMET, G., GARBET, X. & GRANDGIRARD, V. 2009 Shearing effects on density burst propagation in SOL plasmas. *J. Nucl. Mater.* **390-391**, 425.

GIACOMIN, M., STAGNI, A., RICCI, P., BOEDO, J.A., HORACEK, J., REIMERDES, H. & TSUI, C.K. 2021 Theory-based scaling laws of near and far scrape-off layer widths in single-null L-mode discharges. *Nucl. Fusion* **61**, 076002.

GRULKE, O., KLINGER, T., ENDLER, M. & PIEL, A. 2001 Analysis of large-scale fluctuation structures in the scrape-off layer of the Wendelstein 7-AS stellarator. *Phys. Plasmas* **8**, 5171.

HALPERN, F.D., LABOMBARD, B., TERRY, J.L. & ZWEBEN, S.J. 2017 Outer midplane scrape-off layer profiles and turbulence in simulations of Alcator C-Mod inner-wall limited discharges. *Phys. Plasmas* **24**, 072502.

HAPPEL, T., GREINER, F., MAHDIZADEH, N., NOLD, B., RAMISCH, M. & STROTH, U. 2009 Generation of intermittent turbulent events at the transition from closed to open field lines in a toroidal plasma. *Phys. Rev. Lett.* **102**, 255001.

KATZ, N., EGEDAL, J., FOX, W., LE, A. & PORKOLAB, M. 2008 Experiments on the propagation of plasma filaments. *Phys. Rev. Lett.* **101**, 015003.

KIRK, A., THORNTON, A.J., HARRISON, J.R., MILITELLO, F. & WALKDEN, N.R. 2016 L-mode filament characteristics on MAST as a function of plasma current measured using visible imaging. *Plasma Phys. Control. Fusion* **58**, 085008.

KRASHENINNIKOV, S.I. 2001 On scrape off layer plasma transport. *Phys. Lett.* A **283**, 368.

LABOMBARD, B., BOIVIN, R.L., GREENWALD, M., HUGHES, J. & GROUP, A. 2001 Particle transport in the scrape-off layer and its relationship to discharge density limit in Alcator C-Mod. *Phys. Plasmas* **8**, 2107.

LIN, H., LI, G.X., BENGTSON, R.D., RITZ, C.P. & TSUI, H. 1992 A comparison fluctuations of Langmuir probe techniques for measuring temperature. *Rev. Sci. Instrum.* **63**, 4611.

MILITELLO, F. & OMOTANI, J.T. 2016 Scrape off layer profiles interpreted with filament dynamics. *Nucl. Fusion* **56**, 104004.

MYRA, J.R., D'IPPOLITO, D.A., STOTLER, D.P., ZWEBEN, S.J., LEBLANC, B.P., MENARD, J.E., MAQUEDA, R.J. & BOEDO, J. 2006*a* Blob birth and transport in the tokamak edge plasma: analysis of imaging data. *Phys. Plasmas* **13**, 092509.

MYRA, J.R., RUSSELL, D.A. & D'IPPOLITO, D.A. 2006*b* Collisionality and magnetic geometry effects on tokamak edge turbulent transport. I. A two-region model with application to blobs. *Phys. Plasmas* **13**, 112502.

OFFEDDU, N., HAN, W., THEILER, C., GOLFINOPOULOS, T., TERRY, J.L., MARMAR, E., WÜTHRICH, C., TSUI, C.K., DE OLIVEIRA, H., DUVAL, B.P., GALASSI, D., OLIVEIRA, D.S., MANCINI, D. & THE TCV TEAM 2022 Cross-field and parallel dynamics of SOL filaments in TCV. *Nucl. Fusion* **62**, 096014.

RUSSELL, D.A., MYRA, J.R. & D'IPPOLITO, D.A. 2007 Collisionality and magnetic geometry effects on tokamak edge turbulent transport. II. Many-blob turbulence in the two-region model. *Phys. Plasmas* **14**, 102307.

SHESTERIKOV, I., XU, Y., HIDALGO, C., BERTE, M., DUMORTIER, P., SCHOOR, M.V., VERGOTE, M. & VAN OOST, G. 2012 Direct evidence of eddy breaking and tilting by edge sheared flows observed in the TEXTOR tokamak. *Nucl. Fusion* **52**, 042004.

TERRY, J.L., ZWEBEN, S.J., HALLATSCHEK, K., LABOMBARD, B., MAQUEDA, R.J., BAI, B., BOSWELL, C.J., GREENWALD, M., KOPON, D., NEVINS, W.M., PITCHER, C.S., ROGERS, B.N., STOTLER, D.P. & XU, X.Q. 2003 Observations of the turbulence in the scrape-off-layer of Alcator C-Mod and comparisons with simulation. *Phys. Plasmas* **10**, 1739.

https://doi.org/10.1017/S002237782200112X Published online by Cambridge University Press

Tsui, C.K., Boedo, J.A., Myra, J.R., Duval, B., Labit, B., Theiler, C., Vianello, N., Vijvers, W.A.J., Reimerdes, H., Coda, S., Février, O., Harrison, J.R., Horacek, J., Lipschultz, B., Maurizio, R., Nespoli, F., Sheikh, U., Verhaegh, K. & Walkden, N. 2018 Filamentary velocity scaling validation in the TCV tokamak. *Phys. Plasmas* **25**, 072506.

Tsui, H.Y.W., Bengtson, R.D., Li, G.X., Lin, H., Meier, M., Ritz, C.P. & Wootton, A.J. 1992 A new scheme for Langmuir probe measurement of transport and electron temperature fluctuations. *Rev. Sci. Instrum.* **63**, 4608.

Vianello, N., *et al.* 2019 Scrape-off layer transport and filament characteristics in high-density tokamak regimes. *Nucl. Fusion* **60**, 016001.

Xu, G.S., Naulin, V., Fundamenski, W., Hidalgo, C., Alonso, J.A., Silva, C., Gonçalves, B., Nielsen, A.H., Juul Rasmussen, J., Krasheninnikov, S.I., Wan, B.N. & Stamp, M. 2009 Blob/hole formation and zonal-flow generation in the edge plasma of the JET tokamak. *Nucl. Fusion* **49**, 092002.

Xu, Y.H., Jachmich, S., Weynants, R.R. & the TEXTOR team 2005 On the properties of turbulence intermittency in the boundary of the TEXTOR tokamak. *Plasma Phys. Control. Fusion* **47**, 1841.

Yang, Q.Q., Xu, G., Zhong, F.C., Wang, L., Wang, H.Q., Chen, R., Yan, N., Liu, S.C., Chen, L. & Jia, M.N. 2015 Impact of E $\times$ B flow shear on turbulence and resulting power fall-off width in H-mode plasmas in experimental advanced superconducting tokamak. *Phys. Plasmas* **22**, 062504.

Yu, G.Q. & Krasheninnikov, S.I. 2003 Dynamics of blobs in scrape-off-layer/shadow regions of tokamaks and linear devices. *Phys. Plasmas* **10**, 4413.

Zhang, W., Cziegier, I., Bobkov, V., Conway, G.D., Fuchert, G., Griener, M., Kardaun, O., Manz, P., Noterdaeme, J.M. & Seliunin, E. 2019 Blob distortion by radio-frequency induced sheared flow. *Nucl. Fusion* **59**, 074001.

Zweben, S.J., Maqueda, R.J., Stotler, D.P., Keesee, A., Boedo, J., Bush, C.E., Kaye, S.M., LeBlanc, B., Lowrance, J.L., Mastrocola, V.J., Maingi, R., Nishino, N., Renda, G., Swain, D.W., Wilgen, J.B. & the NSTX Team 2003 High-speed imaging of edge turbulence in NSTX. *Nucl. Fusion* **44**, 134.

https://doi.org/10.1017/S002237782200112X Published online by Cambridge University Press